Aberration-corrected Scanning Transmission Electron Microscopy for Atomic-scale Characterization of Semiconductor Devices

ECS Transactions, 11 (3) 225-231 (2007)
10.1149/1.2779062 ©The Electrochemical Society

Aberration-corrected Scanning Transmission Electron Microscopy for Atomic-scale Characterization of Semiconductor Devices

K. van Benthem[a,b] and S. J. Pennycook[b]

[a] Center for Nanophase Materials Sciences, Oak Ridge National Laboratory, Oak Ridge, TN 37831, USA
[b] Materials Sciences and Technology Division, Oak Ridge National Laboratory, Oak Ridge, TN 37831, USA

Aberration correction in the scanning transmission electron microscope brings sub-Ångström electron probe sizes and single atom sensitivity which enable the characterization of semiconductor devices and their defects with unprecedented detail. Further benefits include simultaneous bright field and dark field image acquisition and a new three-dimensional imaging technique. Here, we will review some major results obtained by aberration corrected scanning transmission electron microscopy and highlight some future research directions.

Introduction

The continuing shrinkage of semiconductor devices (1,2) enforces the urgent need for characterization and diagnostic tools to investigate the atomic and electronic structure of devices at the atomic length scale. Transmission electron microscopy (TEM) is an ideal tool for the investigation of atomic structures of materials and their defects (3,4). When combined with electron energy-loss spectroscopy (EELS), the local chemistry, electronic structure and optical properties can be obtained with unprecedented spatial resolution (5). Scanning transmission electron microscopy (STEM), a special TEM technique, can be used to focus the electron beam into a small probe to obtain atomic and electronic structures from the very small volumes in which the electron beam interacts with the specimen. Only recently, aberration correctors for scanning transmission electron microscopes enabled resolution limits in the sub-Ångström regime (6-8). Consequently, STEM has become a unique characterization tool with single-atom sensitivity to investigate atomic structures even in three dimensions (9-11).

In this paper we will review some basics concepts of STEM and highlight especially recent advances in the field due to the success of aberration correction. Several different results obtained from semiconductor materials will be reviewed as examples for different experimental techniques.

Aberration-corrected STEM

In a dedicated STEM the effective source size of the electron emitter is de-magnified by a condenser lens system and transferred to the objective lens which focuses the beam into a small probe in its back focal plane. There, the small electron probe is rastered across an electron transparent specimen. The electrons transmitted through the specimen can then be recorded by various detectors as a function of probe position on the sample. A sketch view of the experimental setup in a STEM is represented in Figure 1.

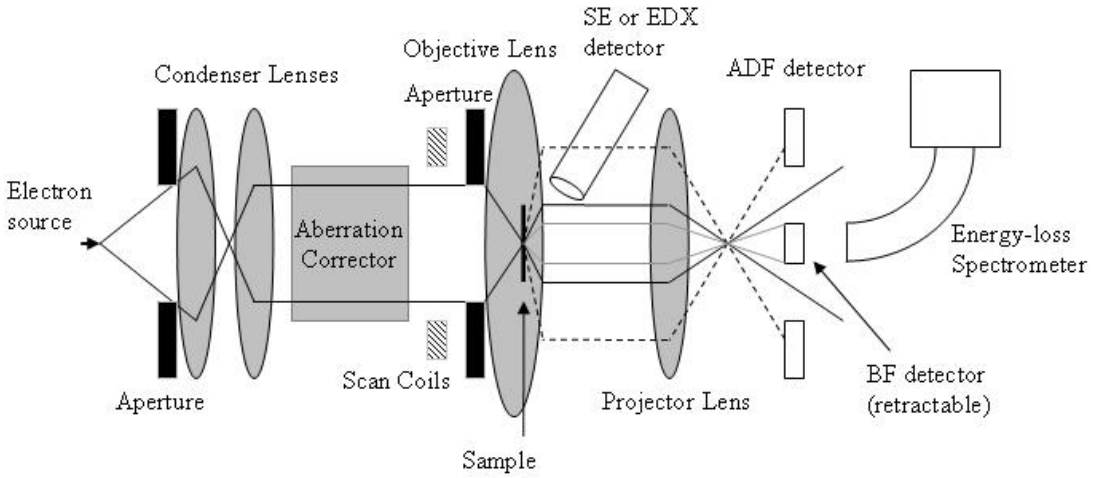

Figure 1. Sketch of an aberration-corrected dedicated scanning transmission electron microscope. Electron trajectories at the edge of the apertures are indicated by solid lines. High angle scattering used for the formation of ADF images is represented by dashed lines while low angle scattering forming aberration-corrected bright field images is indicated by grey lines.

Detectors commonly used in a STEM include annular dark-field (ADF), on-axis bright field (BF) and secondary electron (SE) detectors as well as energy-dispersive X-ray spectrometers (EDX) and energy-loss spectrometers. One of the benefits of a dedicated STEM as illustrated in Figure 1 is that most of the different detector signals can be acquired simultaneously with pixel-to-pixel correlation, provided that their exposure is not geometrically obstructed as in the case of the on-axis detectors. Examples of the simultaneous data acquisition will be presented below.

Based on the theorem of reciprocity (12), a bright field image recorded with a STEM is identical with images recorded by high-resolution TEM (HRTEM), which are based on diffraction interference or phase contrast. Through the use of ADF detectors with a reasonably large inner detector angle, Rutherford scattering by the atomic nuclei is the predominant contrast mechanism. This is an incoherent signal because large detector sizes cause an integration of phase contrast effects, *i.e.*, different Bragg reflections are integrated to form an image based on total scattered intensity. The cross-section is roughly proportional to the square of the atomic number of the scattering element. Hence, this imaging technique is often referred to as *Z*-contrast imaging or high angle ADF (HAADF) imaging. The image formation is incoherent making images directly interpretable without the need of extensive image simulations.

The resolution limiting factor in STEM has historically been the spherical aberration of the probe forming lenses, particularly the objective lens. Third-order aberration correction revolutionized electron microscopy, allowing materials characterization with unprecedented detail, due to the possibility of using electron probe sizes well below 1 Å (6-8). Direct consequences of this development is not only the significantly increased lateral spatial resolution but also an increased signal to noise ratio, enabling single atom sensitivity (13), and higher depth sensitivity providing higher resolution in the vertical direction (10,11,14,15). Several examples demonstrating the effects of aberration correction will be presented and discussed in the following section.

Examples & Discussion

Figure 2 shows two annular dark-field micrographs recorded from a silicon single crystal along its <112> direction using Oak Ridge's VG Microscopes HB603 U and VG501 UX STEM at 300 keV (a) and 100 keV (b), respectively. In Figure 2a the characteristic silicon dumbbell structure is resolved indicating a resolution of 0.78Å (8). However, the micrograph shown in Figure 2b does not quite resolve this spacing. An analysis of the diffractogram revealed [513] spots, *i.e.*, information is transferred to a cut-off of 0.92 Å, which is in agreement with the observed spacing of 0.92±0.04 Å as measured from the acquired images (see Figure 2b). However, both images represent record resolution experiments at the given accelerating voltages, a clear consequence of the applied third-order aberration correction.

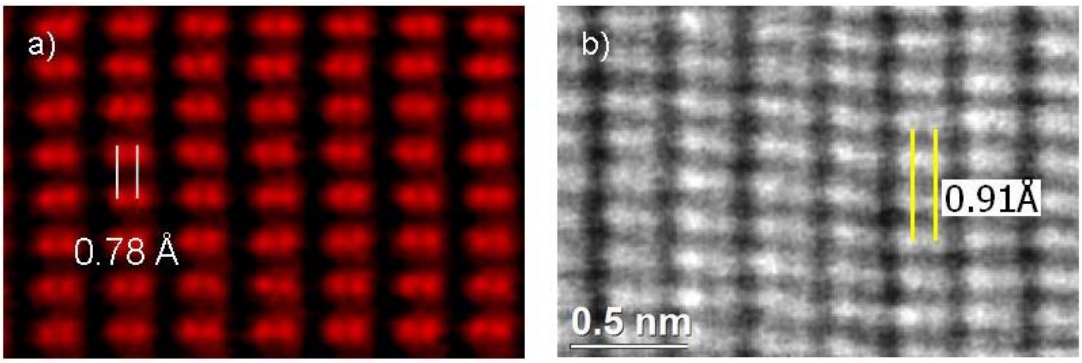

Figure 2. HAADF images of silicon in <112> zone-axis orientation. The micrograph in a) was taken at 300 keV and resolves the 0.78 Å spacing between two adjacent Si columns, adapted from (8). The micrograph in b) was taken at 100 keV, and the Si "dumbbell" structure is not fully resolved.

Based on the theory of reciprocity, a bright field image recorded with a dedicated STEM is equivalent to a conventional phase contrast image recorded with parallel illumination (16). Since only a small fraction of the electrons that are incident upon the sample are admitted by the collector aperture to form the image, the efficiency of BF STEM imaging has traditionally been very low. Aberration correction leads to a decreased gradient of the aberration function (17) so that significantly larger collector apertures can be used. Consequently, bright field imaging becomes more efficient by about two orders of magnitude so that suitable signal to noise ratios can be achieved. The benefit of the STEM imaging mode thereby is that ADF and BF signals can be acquired simultaneously as a function of probe position. Therefore, bright field images, which are sensitive to light elements and *Z*-contrast images can be acquired at the same time with pixel-to-pixel correlation. An example for the simultaneous acquisition of BF and ADF images is shown in Figure 3. The images were recorded from an interface between a thin HfO_2 layer and a silicon substrate grown by atomic-layer deposition. This alternative gate stack was capped with polycrystalline Si after the deposition process. In Figure 3a the ADF image clearly shows the HfO_2 film in bright contrast and the Si substrate in <110> zone-axis orientation with less overall intensity. The relative contrast between the HfO_2 film and the substrate diminishes and no crystalline structure is observable. The BF image in Figure 3b reveals the presence of a strongly disordered, amorphous interlayer of about 0.8 nm thickness between HfO_2 and silicon. Furthermore, the HfO_2 film can be

identified as being polycrystalline. It becomes immediately clear that the simultaneous acquisition of ADF and BF signals reveals additional information which would not have been accessible by recording just one of the signals. Such a type of signal acquisition is beneficial especially for heavy nanomaterials embedded in or supported by light supports, as, for instance, localization of dopant or impurity atoms in semiconductors or in catalysis research.

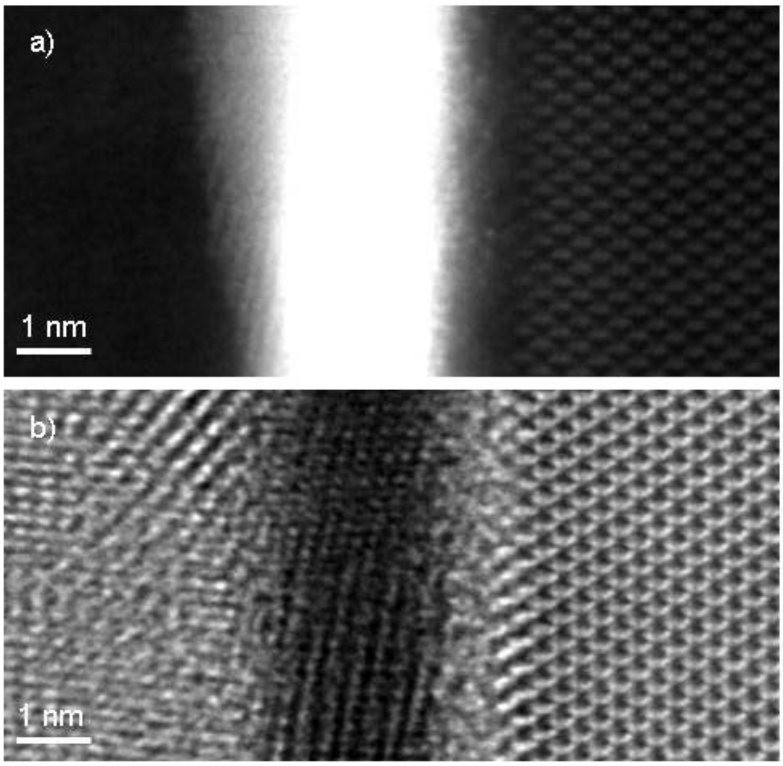

Figure 3. Simultaneously acquired ADF (a) and BF (b) images of a poly-Si/HfO_2/SiO_x/Si alternate gate dielectric stack. Both micrographs were extracted from a figure originally published in references 10 and 11.

When zooming in to the interlayer, electron energy-loss spectroscopy has revealed that this interlayer consists of a silicon oxide. Upon close inspection spots of bright contrast can be observed throughout this interlayer in multiple different positions (10,11). These bright spots have been identified as single Hf atoms embedded in the SiO_x structure (10,11,18,19). Figure 4a shows a Fourier filtered and subsequently color-coded ADF image. Even though the single atoms are observable in the raw data (Figure 3a), such filtering artificially enhances the contrast to make the atoms more visible. However, relative contrast is not conserved after filtering.

Another benefit of aberration correction is a significant decrease in the depth of field *T*, which is given by

$$T = \frac{\delta_s}{\alpha} = \frac{\lambda}{\alpha^2}. \qquad [1]$$

where δ_s represents the probe diameter, α is the illumination semi-angle and λ is the wavelength of the electron beam at the given accelerating voltage. Using aberration

correction smaller electron probe sizes become available through increase of the illumination angle. Therefore, thinner slabs of the TEM sample are in focus at a given defocus and, hence, higher depth sensitivity is achieved. Based on this concept, the acquisition of through focal series effectively becomes equivalent to an optical slicing of the TEM sample. A recorded stack of ADF images can then be used for three dimensional reconstructions of the structure under investigation. In the case of the alternate gate dielectric stack discussed above, it was possible to acquire through-focal series of ADF images. In the recorded image stack single Hf atoms came into focus at different depths. A final reconstruction of the three dimensional interface structure is shown in Figure 4b from which every single Hf atom can be located in three dimensions.

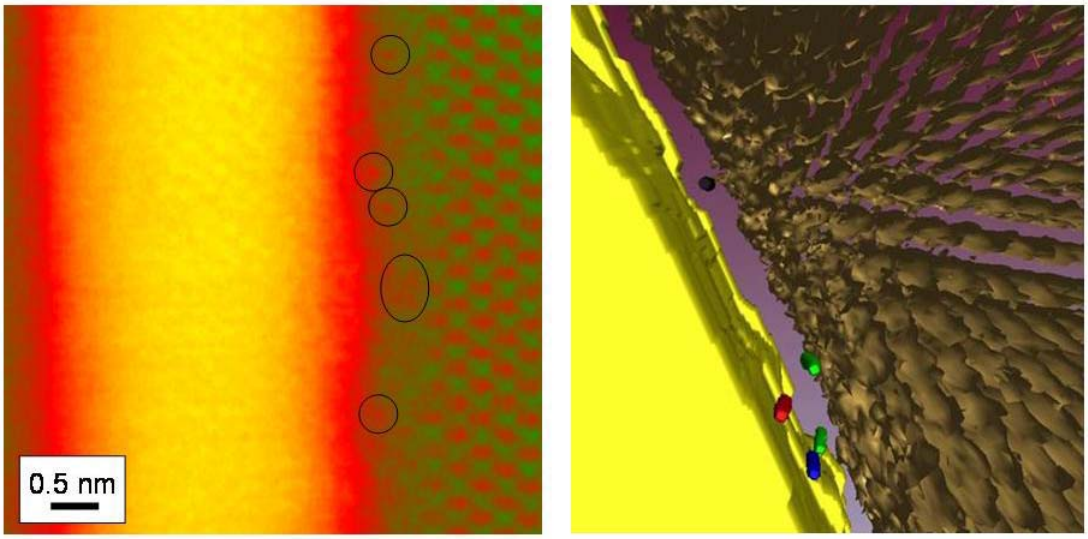

(a) (b)

Figure 4. (a) Fourier filtered and color-coded ADF image of the p-Si/HfO_2/SiO_x/Si interface structure. Single Hf atoms are clearly visible inside the SiO_x interlayer and are encircled; (b) shows a three dimensional reconstruction of the interface obtained from a through-focal series of ADF images. The Si atom columns are shown in gold while the HfO_2 film is colored in bold yellow. This figure was extracted from data published in references 10 and 11. Single Hf atoms are represented by green, blue, red and black colors while the SiO_x film is not colored for clarity.

Although the lateral spatial resolution for ADF imaging in STEM is of the order of 0.78 Å (8), the vertical resolution is under the current imaging conditions only of the order of 7-8 nm, *i.e.*, twice the depth of field (11,15). This anisotropy in the resolution limits leads to the cigar-shaped structure of the single Hf atoms as observed in Figure 4b. To enhance the vertical resolution, deconvolution techniques can be employed to remove effects of the anisotropic point spread function. Such techniques are commonly employed for optical confocal microscopy data and are part of our ongoing research for through-focal series electron microscopy. For "confocal STEM" depth sensitivity is predominantly controlled by significant changes in signal-to-background ratios (SNB) along the vertical direction. For a single Hf atom embedded in an SiO_x matrix the local SNB rises significantly around the vertical position of the Hf atom, leading to the cigar shaped structures identified in Figure 4b. However, the vertical length of the "cigar" is less than the vertical resolution due to a low SNB caused by out-of-focus contributions

from the HfO_2 film and the Si substrate (see, for instance, Figure 7 in reference 11). The SNB of an isolated Hf atom in an extended SiO_x matrix is much higher.

As discussed above, the "confocal STEM" technique is able to reliably locate heavy element structures three-dimensionally when embedded in a light supporting matrix. However, the three-dimensional characterization of the morphology of, for instance, nanocrystals remains inconclusive. In an earlier study (20) isolated Au nanoclusters supported by an amorphous carbon film were imaged by through-focal series acquisition of *Z*-contrast images. Even though single Au atoms could be detected in the vicinity of the nanocrystals, a true three-dimensional reconstruction of the crystals morphology could not be obtained. Instead, a quantitative analysis of image intensities combined with ADF image simulations revealed the number of Au atoms in each column of the nanocrystals. Hence, information on the number of atoms per crystal was obtained. Faceting of the nanocrystals can be assumed based on the atom count, but could not be imaged directly. In future studies, a combination of through-focal series acquisition and discrete tilt-series tomography is expected to overcome these limitations so that crystal structures and morphologies can be determined with atomic resolution and single atom sensitivity.

Conclusions

Aberration corrected STEM offers sub-Ångström electron probe sizes and single atom sensitivity so that materials and their defects can be characterized with unprecedented detail. Further consequences include the simultaneous acquisition of *Z*-contrast and bright field images with reasonable signal-to-background ratios so that maximal information from both heavy element structures and their light-element support can be deduced. The availability of larger probe forming angles due to aberration correction leads to significantly increased depth sensitivity and, therefore, enables a new three-dimensional imaging technique by through-focal series acquisition. Single dopant and impurity atoms can be located within defect structures with high precision and reliability.

Acknowledgments

This research was sponsored by the Office of Basic Energy Sciences, Division of Materials Sciences and Engineering, U.S. Department of Energy and by appointment to the ORNL Postdoctoral Research Program administered jointly by ORNL and ORISE. The authors are grateful to J.T. Luck for excellent specimen preparation and acknowledge fruitful discussions with the following colleagues: A. Marinopoulos, S.T. Pantelides, M.P. Oxley, S.D. Findlay, L.J. Allen, A.R. Lupini, and A.Y. Borisevich.

References

1. P.D. Moore, *Electronics* **38** (1965)
2. P.A. Packan, *Science* **285**, 2079 (1999)
3. L. Reimer, Transmission Electron Microscopy, Springer Berlin, Heidelberg, New York, 4th edition (1997)
4. D.B. Williams and C.B. Carter, Transmission Electron Microscopy, Plenum Press, New York and London (1996)
5. R. F. Egerton, Electron Energy-Loss Spectroscopy in the Electron Microscope, Plenum Press, New York and London, 2nd edition (1996)

6. P.E. Batson, N. Delby, and O. L. Krivaneck, *Nature* **418**, 617 (2002)
7. O.L. Krivanek, P.D. Nellist, N. Dellby, M.F. Murfitt, Z. Szilagyi, *Ultramicroscopy* **96**, 229 (2003)
8. K. van Benthem, Y. Peng and S. J. Pennycook, *Mat. Res. Soc. Symp. Proc.* **839**, 3 (2005)
9. P.D. Nellist *et al.*, *Science* **305**, 1741 (2004)
10. K. van Benthem et al., *Appl. Phys. Lett.* **87**, 034104 (2005)
11. K. van Benthem et al., *Ultramicroscopy* **106**, 1062 (2006)
12. Cowley, J.M., *Appl. Phys. Lett.* **15**, 58 (1969)
13. S. Wang *et al.*, *Nature Materials* **3**, 143 (2004).
14. A.Y. Borisevich *et al.*, *J Electron Microsc.* **55**, 7 (2006)
15. A.Y. Borisevich, A.R. Lupini, S.J. Pennycook, *Proc. Natl. Acad. Sci.* **103**, 19212 (2006)
16. M. Varela *et al.*, *Annual Review of Materials Research 2005* **35**, 539 (2005)
17. J. Frank, *Optik* **38**, 519 (1973)
18. D.O. Klenov, T.E. Mates and S. Stemmer, *Appl. Phys. Lett.* **89**, 041918 (2006)
19. P. E. Batson, *Microsc. Microanal.* **11** (Suppl 2), 2124 (2005).
20. K. van Benthem, Y. Peng, S.J. Pennycook, *Mat. Res. Soc. Symp. Proc.* **839**, 3 (2005)